Ore Geology Reviews 78 (2016) 166–175

Contents lists available at ScienceDirect

Ore Geology Reviews

journal homepage: www.elsevier.com/locate/oregeorev

Chemical composition and evolution of the garnets in the Astamal Fe-LREE distal skarn deposit, Qara-Dagh–Sabalan metallogenic belt, Lesser Caucasus, NW Iran

Saeid Baghban [a,*], Mohammad Reza Hosseinzadeh [a], Mohsen Moayyed [a], Mir Ali Asghar Mokhtari [b], Daniel David Gregory [c], Hosein Mahmoudi Nia [a]

[a] Department of Earth Sciences, Faculty of Natural Sciences, University of Tabriz, 5166616471 Tabriz, Iran
[b] Department of Geology, Faculty of Science, University of Zanjan, 45371-38791 Zanjan, Iran
[c] ARC Centre of Excellence in Ore Deposits (CODES), School of Physical Sciences, University of Tasmania, Private Bag 79, Hobart, Tasmania 7001, Australia

ARTICLE INFO

Article history:
Received 24 September 2015
Received in revised form 26 February 2016
Accepted 29 February 2016
Available online 29 March 2016

Keywords:
NW Iran
Astamal
Distal skarn
Garnet
Chemical zoning
Discrete grossular-almandine-rich domains
Mineral chemistry

ABSTRACT

The chemistry of garnet can provide clues to the formation of skarn deposits. The chemical analyses of garnets from the Astamal Fe-LREE distal skarn deposit were completed using an electron probe micro-analyzer. The three types of garnet were identified in the Astamal skarn are: (I) euhedral coarse-grained isotropic garnets (10–30 mm across), which are strongly altered to epidote, calcite and quartz in their rim and core, with intense pervasive retrograde alteration and little variation in the overall composition ($Adr_{94.3-84.4}$ $Grs_{8.5-2.7}$ $Alm_{1.9-0.2}$) (garnet I); (II) anhedral to subhedral brecciated isotropic garnets (5–10 mm across) with minor alteration, a narrow compositional range along the growth lines ($Adr_{82-65.4}$ $Grs_{21.9-11.7}$ $Alm_{11.1-2.4}$) and relatively high Cu (up to 1997 ppm) and Ni (up to 1283 ppm) (garnet II); and (III) subhedral coarser grained garnets (>30 mm across) with moderate alteration, weak diffusion and irregular zoning of discrete grossular-almandine-rich domains ($Adr_{84.2-48.8}$ $Grs_{32.4-7.6}$ $Alm_{19.9-3.5}$) (garnet III). In the third type, the almandine content increases with increasing grossular/andradite ratio and increasing substitutions of Al for Fe^{3+}.
Almost all three garnet types have been replaced by fine-grained, dark-brown allanite that is typically disseminated and has the same relief as andradite. The Cu content increases while Ni content decreases slightly towards the rim of garnet II and garnet III. Copper in garnet II is positively correlated with increasing almandine content and decreasing andradite content, indicating that the almandine structure, containing relatively more Fe^{2+}, is more suitable than andradite and grossular to host divalent cations such as Cu^{2+}. Nickel in garnet II is positively correlated with increasing andradite content, total Fe, and decreasing almandine content. This is because Ni^{2+} substitutes for Fe^{3+} in the Y (octahedral) position. There are unusual discrete grossular-almandine rich domains within andraditic garnet III, indicating the low diffusivity of Ca compared to Fe at high temperatures.

1. Introduction

Garnet is a common rock-forming mineral in many skarn deposits, with a variety of compositions that allow it to be utilized in studying ore-forming processes and aid in ore deposit exploration (e.g., Jamtveit and Hervig, 1994; Whitney and Olmsted, 1998; Nicolescu et al., 1998; Karimzadeh Somarin, 2004, 2010; Smith et al., 2004; Gaspar et al., 2008; Ismail et al., 2014; Peng et al., 2015). The majority of skarn deposits are spatially related to the emplacement of intrusions, thus the minerals within a skarn can provide a record of the hydrothermal fluids present during ore formation (Meinert et al., 2005). In other words, the evolution of a fluid's composition may be recorded in the mineral growth zones of garnets, particularly in skarn bodies where the growth of garnet reflects the interplay between heat and fluid infiltration (e.g. Jamtveit, 1997). Meinert et al. (2005) described the compositional variation of garnet during the passage of an alteration front in which systematic zonation patterns differ with proximity to the fluid source. In more complex systems with evolving and cyclical fluid flow patterns that cannot be distinguished or separated, the interpretation of skarn zonation is more difficult (Meinert et al., 2005). In these systems, chemical zonation in garnets record the evolution of the deposit in terms of temperature variation, rate of fluid flow, compositional variation of mineralizing hydrothermal fluids, and the oxidation state of hydrothermal fluids.

The Astamal Fe-LREE skarn deposit is located approximately 85 km north of Tabriz, in the Qara-Dagh ore district of the Lesser Caucasus in the Alpine–Himalayan Orogen of northwestern Iran (Fig. 1). The

* Corresponding author at: Abrasan Street, Pezeshkan-Plaque 1.17, Postal Code: 5156845714, Tabriz, Iran.
E-mail addresses: Saeid.Baghban_geomine@yahoo.com, SaeidBaghban@gmail.com (S. Baghban).

http://dx.doi.org/10.1016/j.oregeorev.2016.02.020
0169-1368/

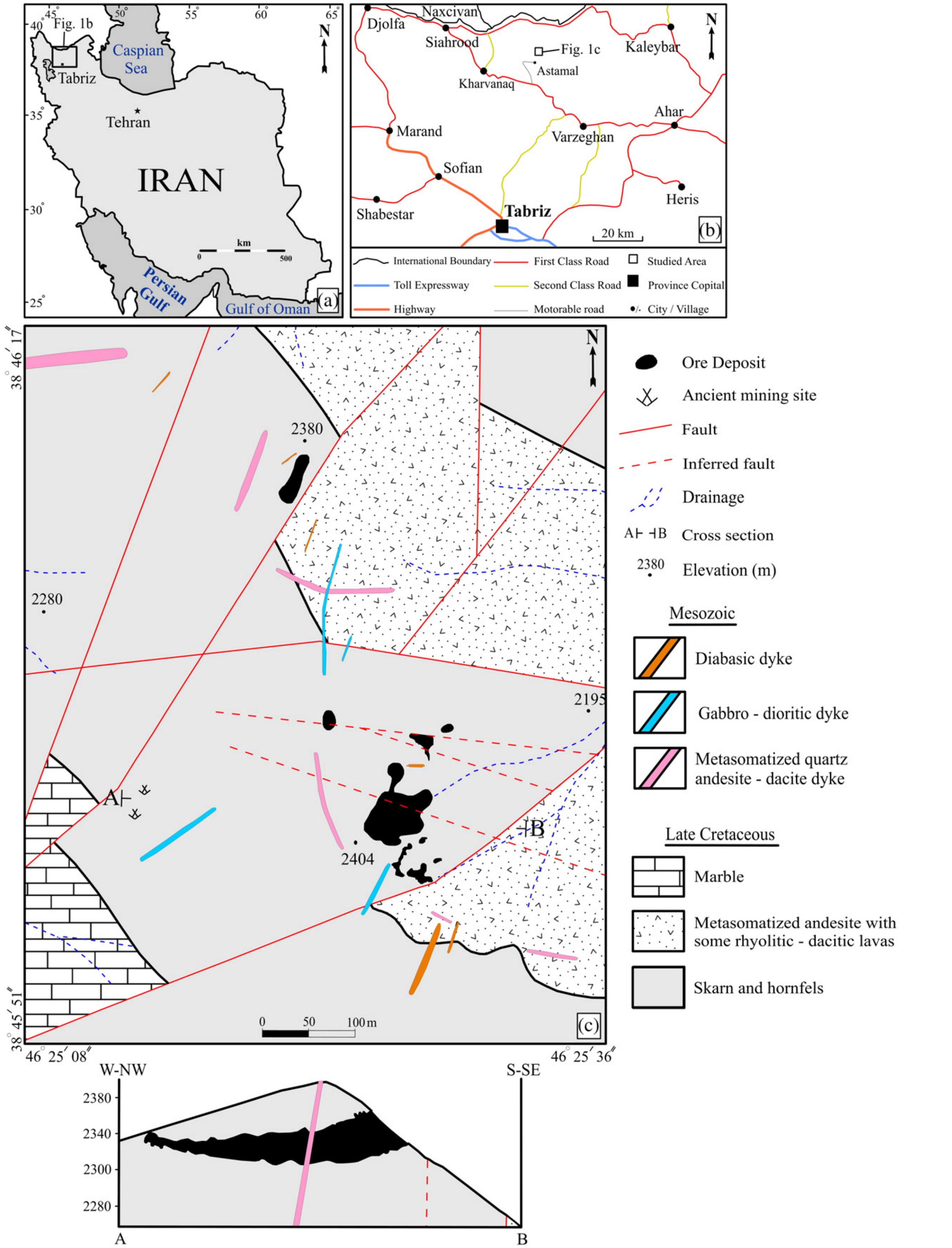

Fig 1. Detailed geological map of the Astamal skarn deposit (Baghban et al., 2015).

Geological Survey of Iran (GSI) recently discovered the mineralization in the area and Astamal is the largest and richest magnetite deposit with a resource of >10 Mt magnetite grading ~60% Fe (Mokhtari and Hosseinzadeh, 2013). Baghban et al. (2015) give detailed descriptions of the geological characteristics of the Fe ore and skarn bodies, the formation conditions of calc-silicate minerals, and descriptions of light

Table 1
Garnet EPMA data from the Astamal skarn deposit.

Sample	A 12			A 13			A 14			A 15			A16		A17	
Comment	Core		Rim	Core		Rim	Core		Rim	Core		Rim	Core	Rim	Core	Rim
Major oxides, weight percent																
SiO_2	35.49	35.59	35.11	35.72	35.72	35.59	35.63	35.98	35.94	36.05	36.34	36.38	36.25	36.88	36.83	37.14
TiO_2	0.07	0.16	0.61	0.17	0.35	0.82	0.11	0.14	0.67	0.30	0.12	0.26	0.52	0.56	0.41	0.52
Al_2O_3	0.88	1.20	1.37	0.61	0.83	1.62	1.32	1.70	1.94	2.71	2.98	3.26	4.11	4.53	3.55	3.98
Cr_2O_3	0.02	0.00	0.01	0.03	0.01	0.03	0.02	0.00	0.06	0.04	0.02	0.02	0.00	0.00	0.01	0.03
FeO[a]	30.39	30.05	29.97	29.96	29.56	28.61	29.51	28.92	27.98	27.92	27.66	27.12	27.24	26.34	27.78	27.07
MnO	0.69	0.81	0.94	0.76	0.98	1.23	0.88	1.07	1.06	0.68	0.77	0.75	0.97	1.10	0.96	1.07
MgO	0.11	0.13	0.20	0.18	0.43	0.59	0.19	0.31	0.67	0.54	0.52	0.53	0.33	0.54	0.83	0.95
CaO	32.36	31.97	31.55	32.48	31.91	31.43	32.29	31.97	31.66	31.76	31.42	31.64	30.54	29.96	29.56	29.06
Na_2O	0.01	0.00	0.02	0.00	0.03	0.03	0.02	0.01	0.02	0.01	0.16	0.05	0.05	0.09	0.05	0.07
K_2O	0.01	0.01	0.01	0.00	0.00	0.00	0.00	0.00	0.00	0.00	0.00	0.00	0.06	0.06	0.03	0.04
Total	100.03	99.92	99.79	99.91	99.82	99.95	99.97	100.10	100.00	100.01	99.99	100.01	100.07	100.06	100.01	99.93
Number of ions on the basis of 12 oxygen atoms and garnet end-members normative calculation																
Si	2.914	2.924	2.891	2.935	2.935	2.915	2.921	2.940	2.934	2.935	2.961	2.957	2.950	2.995	2.998	3.021
Ti	0.004	0.010	0.038	0.011	0.022	0.051	0.007	0.009	0.041	0.018	0.007	0.016	0.032	0.034	0.025	0.032
Al	0.085	0.116	0.133	0.059	0.080	0.156	0.128	0.164	0.187	0.260	0.286	0.312	0.394	0.434	0.341	0.382
Cr	0.001	0.000	0.001	0.002	0.001	0.002	0.001	0.000	0.004	0.003	0.001	0.001	0.000	0.000	0.001	0.002
Fe^{3+}[b]	2.074	2.016	2.004	2.048	2.000	1.905	2.013	1.937	1.856	1.829	1.751	1.734	1.628	1.487	1.602	1.495
Fe^{2+}	0.013	0.048	0.059	0.011	0.031	0.055	0.010	0.039	0.054	0.072	0.134	0.109	0.226	0.302	0.289	0.346
Mn	0.048	0.056	0.066	0.053	0.068	0.085	0.061	0.074	0.073	0.047	0.053	0.052	0.067	0.076	0.066	0.074
Mg	0.013	0.016	0.025	0.022	0.053	0.072	0.023	0.038	0.082	0.066	0.063	0.064	0.040	0.065	0.101	0.115
Ca	2.847	2.814	2.784	2.860	2.810	2.759	2.836	2.799	2.769	2.771	2.743	2.755	2.663	2.607	2.578	2.533
Na	0.001	0.000	0.002	0.000	0.002	0.002	0.002	0.001	0.002	0.001	0.013	0.004	0.004	0.007	0.004	0.006
K	0.001	0.001	0.001	0.000	0.000	0.000	0.000	0.000	0.000	0.000	0.000	0.000	0.003	0.003	0.002	0.002
Total	8.000	8.000	8.000	8.000	8.000	8.000	8.000	8.000	8.000	8.000	8.000	8.000	8.000	8.000	8.000	8.000
Almandine	0.43	1.65	2.03	0.38	1.06	1.84	0.35	1.33	1.82	2.44	4.49	3.67	7.55	9.89	9.53	11.29
Spessartine	1.64	1.92	2.24	1.80	2.30	2.87	2.08	2.51	2.46	1.59	1.78	1.73	2.23	2.48	2.18	2.40
Pyrope	0.46	0.54	0.84	0.75	1.78	2.43	0.79	1.28	2.74	2.22	2.11	2.15	1.34	2.14	3.32	3.75
Grossular	3.84	5.22	5.90	2.72	3.66	7.04	5.76	7.39	8.48	11.66	12.87	14.10	17.33	19.30	14.89	16.77
Andradite	93.56	90.66	88.97	94.27	91.17	85.73	90.95	87.48	84.33	81.99	78.70	78.29	71.55	66.19	70.05	65.70
Uvarovite	0.06	0.00	0.03	0.09	0.03	0.09	0.06	0.00	0.18	0.12	0.06	0.06	0.00	0.00	0.03	0.08
Fe/(Fe + Al)	0.961	0.947	0.940	0.972	0.962	0.926	0.941	0.923	0.910	0.879	0.866	0.853	0.824	0.797	0.840	0.818
X_{Fe}	0.994	0.992	0.988	0.989	0.975	0.965	0.989	0.981	0.959	0.967	0.968	0.966	0.979	0.965	0.949	0.941
Trace elements, parts per million																
Cu	bdl	bdl	bdl	bdl	bdl	bdl	bdl	bdl	bdl	479	639	719	1278	1757	1039	1278
Ni	bdl	bdl	bdl	bdl	bdl	bdl	bdl	bdl	bdl	550	393	314	393	314	236	79
Zn	bdl	bdl	bdl	bdl	bdl	bdl	bdl	bdl	bdl	80	241	bdl	bdl	bdl	bdl	161
Zr	bdl	bdl	222	148	74	bdl	bdl	bdl	bdl	bdl	bdl	bdl	bdl	bdl	bdl	bdl
Rb	366	274	bdl	bdl	91	183	bdl	bdl	366	bdl	bdl	bdl	bdl	bdl	bdl	bdl
Sr	169	254	169	423	bdl	338	85	676	bdl	bdl	bdl	bdl	592	bdl	bdl	bdl

Sample	A 30			A38		A 42			A 43			A 44		
Comment	Core		Rim	Core	Rim	Core		Rim	Core		Rim	Core		Rim
Major oxides, weight percent														
SiO_2	36.58	36.79	37.16	36.48	36.73	37.10	37.82	37.06	37.02	38.36	37.29	35.79	38.43	36.02
TiO_2	0.28	0.26	0.26	0.21	0.18	0.04	0.11	0.10	0.12	0.17	0.00	0.30	0.36	0.40
Al_2O_3	3.58	3.91	4.28	4.53	5.25	2.43	6.32	2.52	2.06	7.57	2.33	1.80	6.62	2.39
Cr_2O_3	0.06	0.05	0.02	0.09	0.00	0.04	0.05	0.06	0.02	0.00	0.08	0.04	0.05	0.06
FeO[a]	27.98	27.79	27.11	26.11	25.94	29.12	27.31	29.52	28.48	23.35	28.26	29.71	24.62	29.24
MnO	0.86	1.06	1.20	0.98	1.23	0.41	0.39	0.43	0.49	0.94	0.53	0.76	0.84	0.89
MgO	0.67	0.41	0.73	0.25	0.21	0.50	0.06	0.19	0.06	0.23	0.14	0.67	0.69	0.76
CaO	29.95	29.69	29.11	31.37	30.43	30.41	27.94	30.10	31.63	29.17	31.34	30.89	28.34	30.17
Na_2O	0.02	0.03	0.12	0.03	0.03	0.00	0.02	0.04	0.10	0.18	0.02	0.02	0.03	0.06
K_2O	0.00	0.01	0.00	0.00	0.04	0.00	0.02	0.00	0.04	0.02	0.00	0.00	0.00	0.00
Total	99.98	100.00	99.99	100.05	100.04	100.05	100.04	100.02	100.02	99.99	99.99	99.98	99.98	99.99
Number of ions on the basis of 12 oxygen atoms and garnet end-members normative calculation														
Si	2.978	2.997	3.022	2.957	2.977	3.027	3.069	3.033	3.029	3.089	3.045	2.929	3.098	2.945
Ti	0.017	0.016	0.016	0.013	0.011	0.002	0.007	0.006	0.007	0.010	0.000	0.018	0.022	0.025
Al	0.343	0.375	0.410	0.433	0.501	0.234	0.604	0.243	0.199	0.719	0.224	0.174	0.629	0.230
Cr	0.004	0.003	0.001	0.006	0.000	0.003	0.003	0.004	0.001	0.000	0.005	0.003	0.003	0.004
Fe^{3+}[b]	1.660	1.589	1.494	1.617	1.514	1.705	1.236	1.668	1.707	1.052	1.677	1.926	1.123	1.817
Fe^{2+}	0.245	0.304	0.349	0.153	0.244	0.282	0.618	0.353	0.242	0.521	0.252	0.108	0.536	0.182
Mn	0.059	0.073	0.083	0.067	0.084	0.028	0.027	0.030	0.034	0.064	0.037	0.053	0.057	0.062
Mg	0.081	0.050	0.088	0.030	0.025	0.061	0.007	0.023	0.007	0.028	0.017	0.082	0.083	0.093
Ca	2.612	2.592	2.536	2.724	2.643	2.658	2.429	2.640	2.773	2.517	2.742	2.709	2.448	2.643
Na	0.002	0.002	0.009	0.002	0.002	0.000	0.002	0.003	0.008	0.014	0.002	0.002	0.002	0.005
K	0.000	0.001	0.000	0.000	0.002	0.000	0.001	0.000	0.002	0.001	0.000	0.000	0.000	0.000
Total	8.000	8.000	8.000	8.000	8.000	8.000	8.000	8.000	8.000	8.000	8.000	8.000	8.000	8.000
Almandine	8.18	10.08	11.42	5.13	8.16	9.30	20.05	11.59	7.93	16.65	8.28	3.65	17.17	6.11
Spessartine	1.98	2.42	2.70	2.26	2.82	0.94	0.87	0.98	1.11	2.05	1.20	1.79	1.84	2.07

Number of ions on the basis of 12 oxygen atoms and garnet end-member normative calculation

Table 1 (*continued*)

Sample	A 30			A38		A 42			A 43			A 44		
Comment	Core		Rim	Core	Rim	Core		Rim	Core		Rim	Core		Rim
Pyrope	2.71	1.65	2.90	1.02	0.85	2.01	0.24	0.76	0.24	0.88	0.56	2.77	2.65	3.11
Grossular	14.91	16.38	17.86	19.28	21.94	10.56	25.85	11.00	9.45	32.64	10.58	7.58	28.07	9.96
Andradite	72.05	69.33	65.06	72.06	66.24	77.07	52.86	75.49	81.21	47.78	79.13	84.10	50.13	78.59
Uvarovite	0.17	0.14	0.06	0.26	0.00	0.12	0.14	0.18	0.06	0.00	0.24	0.11	0.14	0.17
Fe/(Fe + Al)	0.842	0.827	0.807	0.797	0.781	0.899	0.748	0.892	0.911	0.664	0.900	0.920	0.694	0.894
X_{Fe}	0.959	0.974	0.954	0.983	0.986	0.970	0.996	0.989	0.996	0.983	0.991	0.961	0.952	0.956
Trace elements, parts per million														
Cu	879	959	1118	1198	1997	bdl	bdl	bdl	80	bdl	bdl	240	bdl	bdl
Ni	bdl	bdl	393	236	157	707	bdl	472	1179	bdl	bdl	1283	bdl	1187
Zn	bdl	bdl	bdl	bdl	bdl	bdl	bdl	bdl	bdl	bdl	bdl	bdl	bdl	bdl
Zr	bdl	bdl	bdl	bdl	bdl	bdl	bdl	bdl	bdl	bdl	bdl	bdl	bdl	bdl
Rb	bdl	bdl	bdl	bdl	bdl	bdl	bdl	bdl	bdl	bdl	bdl	bdl	bdl	bdl
Sr	bdl	bdl	bdl	507	254	bdl	bdl	bdl	bdl	bdl	bdl	bdl	bdl	bdl

bdl = below detection limit.
[a] Total iron as FeO.
[b] Recalculated from stoichiometry.

rare earth elements (LREEs) mineralization throughout the Fe ore and the skarn bodies. However, no detailed information is available on the chemistry and genesis of the garnet.

Garnet is the principal component of skarn at Astamal and this study focuses on the detailed petrography and chemical variation of garnets associated with the mineralization. Baghban et al. (2015) document a broad description of the garnets in the deposit, but our contribution provides a more detailed description of garnets at the deposit. This contribution focuses on the chemical evolution of garnets at Astamal and factors controlling their regular and irregular zonation and Cu and Ni contents. The study helps understand the evolution of the distal skarn deposits at Astamal, providing a better opportunity to decipher the skarn formation processes. Although the chemistry of garnet in a skarn deposit is not the only key to its genesis, the garnet composition is a relatively unique fingerprint and serves as an additional tool in determining the genesis of a skarn.

2. Geological background

The Astamal Fe-LREE skarn deposit is located in the Eastern Azarbaijan Province and is the largest Fe deposit of northwest Iran (Mokhtari and Hosseinzadeh, 2013). Late Cretaceous submarine andesitic volcanics are the most common rocks in the Astamal area. However, Late Cretaceous sedimentary rocks consisting of a flysch-type assemblage are also widespread. This assemblage includes alternating thin- to medium-bedded sandstone, shale, marl and conglomerate covered by thickly bedded to massive limestone (Baghban et al., 2015). Intrusion of the Oligo-Miocene Qara-Dagh Batholith into the Late Cretaceous volcano-sedimentary sequences in the region resulted in widespread contact metamorphism and alteration. Astamal is one of several skarn deposits formed in the region at that time (Fig. 1). The deposit is a distal skarn deposit that outcrops ~600 m to the south-southwest of the granodiorite batholith, which is interpreted to be the source of the fluids that formed the deposit. Astamal is hosted by fractures and faults cutting the volcano-sedimentary rocks, which have acted as conduits for the mineralizing fluids (Baghban et al., 2015).

Four Fe orebodies have been delineated at Astamal. The southern-most Fe orebody is the main orebody with a volume of around 3,500,000 m^3 (200 × 250 × 70 m) hosted by skarn and hornfels. The northern iron orebody is around 20,000 m^3 (10 × 50 × 40 m) and is hosted by calc-silicate hornfels and is situated ~400 m north of the southern-most orebody. The eastern Fe ore body is approximately 1 km east of the main ore body and is poorly exposed (Baghban et al., 2015).

The Fe mineralization at Astamal is predominantly a high-grade massive magnetite deposit, though both minor disseminations and low-grade veins are also present. Pyrrhotite, pyrite, chalcopyrite and minor hematite, malachite, azurite and secondary iron oxide-hydroxide are also present, and Baghban et al. (2015) recognised light rare earth elements (LREEs) at the deposit. The LREE-bearing mineralization is primarily present in epidote, which is most common in the skarn and the Fe-ore zones. The skarn minerals include garnet, epidote, actinolite, calcite, quartz, clinopyroxene and chlorite (in order of abundance; Baghban, 2013).

3. Method of investigation

Thirty-six samples were collected from the skarn zone at Astamal for petrographic and geochemical studies. Petrographic studies (including recognition of mineral assemblages, alteration, metasomatic replacements and textures) were performed using an Olympus BX60 microscope at the ore-deposit laboratory at the University of Tabriz. Based on optical microscope observations, 8 relatively unaltered and 3 altered samples were selected for electron probe micro-analysis (EPMA). The major oxide compositions of the garnets were determined at the mineralogy division of the Iranian Mineral Processing Research Center (IMPRC) using a Cameca SX-100 electron microprobe equipped with 5 wavelength-dispersive crystal spectrometers, operating with a 3 μm beam diameter, 15 kv accelerating voltage, 15 nA sample current and 60 s counting time. The X-ray lines used for all elements in Table 1 were K-α. Elements were calibrated against synthetic and natural standards including: andradite (for Ca and Si), albite (for Na), corundum (for Al), orthoclase (for K), MgO (for Mg), Fe_2O_3 (for Fe), $MnTiO_3$ (for Mn and Ti), Cr_2O_3 (for Cr), ZnS (for Zn), SrO (for Sr), ZrO_2 (for Zr), NiO (for Ni), Cu (for Cu) and rubidium microcline (for Rb). Lower detection limits were calculated to be on the order of 0.01 wt% for all elements. Chemical formulae and end-member proportions for the minerals analyzed were calculated following the method of Deer et al. (1992) and Fe (III) was calculated based on ideal stoichiometric composition. Total Fe (ferrous and ferric) was also used for calculating ratios such as Fe/(Fe + Al) and X_{Fe} [=Fe/(Fe + Mg)]. Representative garnet analyses are given in Table 1.

4. Petrographic observations

The most common minerals observed at the Astamal skarn are, in order of abundance, garnet, epidote, actinolite, allanite, calcite, quartz, clinopyroxene and chlorite. These mineral assemblages occur in a variety of textures, e.g., granoblastic, grano-nematoblastic, poikiloblastic, mega-porphyroblastic, and hornfelsic. In some areas, these minerals have undergone cataclastic deformation and are locally mylonitized (Baghban et al., 2015). Baghban et al. (2015) provide detailed

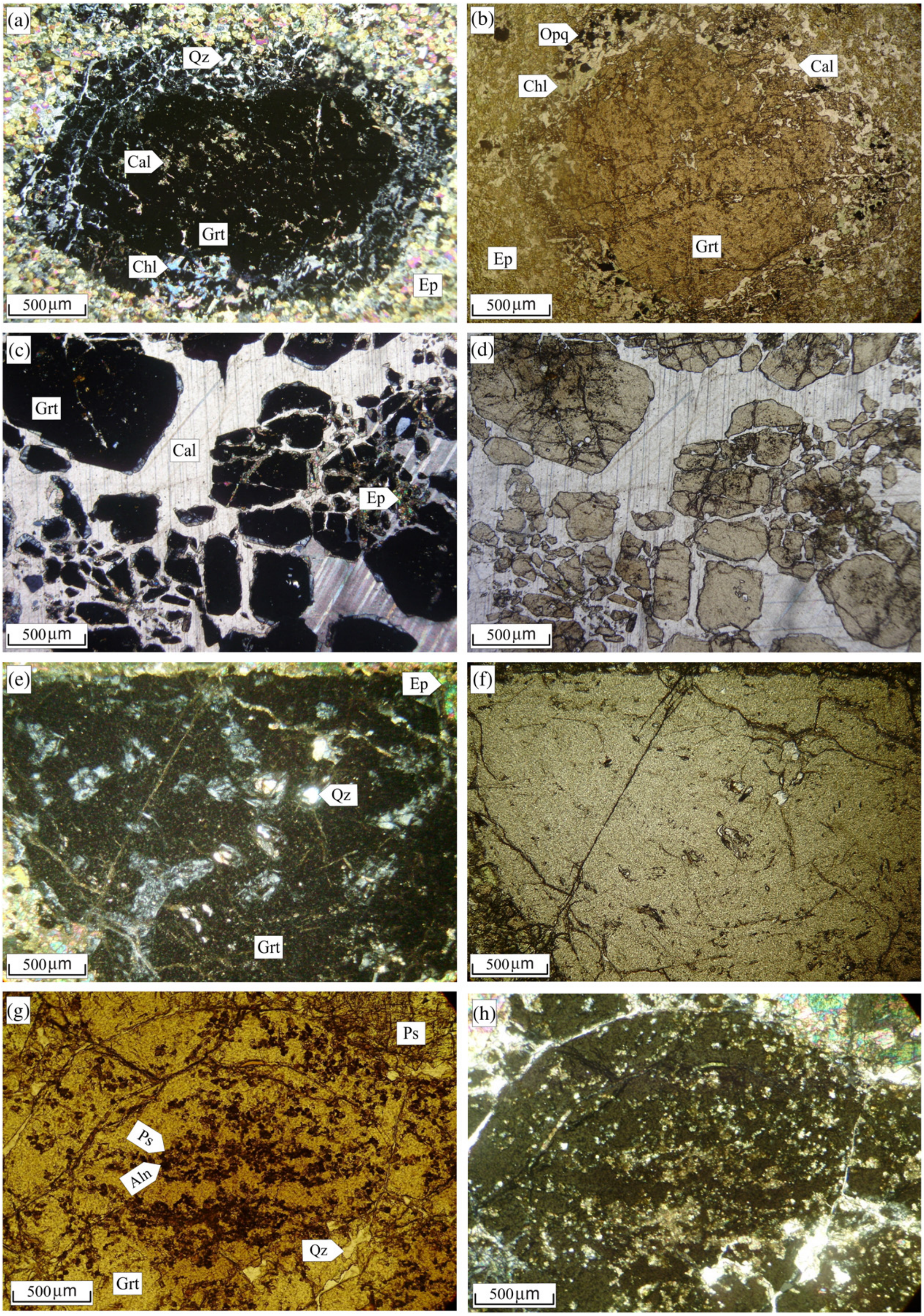
(a)
Qz
Cal
Grt
Chl
Ep
500μm
(b)
Opq
Cal
Chl
Ep
Grt
500μm
(c)
Grt
Cal
Ep
500μm
(d)
500μm
(e)
Ep
Qz
Grt
500μm
(f)
500μm
(g)
Ps
Ps
Aln
Qz
Grt
500μm
(h)
500μm

petrographic and textural observations of the skarn, hornfels and marble zones in the Astamal deposit.

There are 3 types of garnet in the Astamal skarn. Type I are euhedral coarse-grained isotropic garnets (10–30 mm across) that have been intensely retrograde altered to epidote, calcite and quartz, both in the rim and the core (Fig. 2a). Magnetite is observed to replace the rims of this type of garnet and within fissures in the unmineralized skarn zone (Fig. 2b). Type II are anhedral to subhedral isotropic garnets (5–10 mm) that are often brecciated with minor alteration (Fig. 2c–d), while type III are subhedral coarser-grained garnets (>30 mm) that are commonly moderately altered and show weak diffusion and irregular zoning (Fig. 2e–f). The mineral assemblages of retrograde alteration for all three garnet types also include allanite (Fig. 2g–h). The fine-grained, dark-brown allanite is disseminated and has the same relief as andradite. This replacement of garnet by allanite has not been reported in any skarn deposit, though individual crystals have been described in some Fe skarns in Sweden (Jansson and Allen, 2013) and the Astamal skarn deposit (Baghban et al., 2015). The fine-grained, light-brown disseminated pistacite with lower relief can also be observed within the andradite. Due to the intense alteration of garnet I rather than other garnet types, it is interpreted that garnet I has been more influenced by hydrothermal fluids and consequently it is interpreted to have formed earlier than garnet II and garnet III.

5. Mineral chemistry

The EPMA results, mineral formulae and end-member compositions of the different kinds of garnet crystals from the Astamal skarn are given in Table 1. Garnet I (samples A12, A13 and A14), which is generally isotropic, has no specific zoning along the growth lines and falls within a narrow compositional range ($Adr_{94.27–84.33}$ $Grs_{8.48–2.72}$ $Alm_{2.03–0.35}$). Garnet II (samples A15, A16, A17, A30 and A38) has relatively low andradite content compared to garnet I, little variation in composition ($Adr_{94.3–84.4}$ $Grs_{8.5–2.7}$ $Alm_{1.9–0.2}$) and discernible Cu and Ni content. In contrast to type I and II garnets, garnet III (samples A42, A43 and A44) has considerable variation in composition ($Adr_{84.2–48.8}$ $Grs_{32.4–7.6}$ $Alm_{19.9–3.5}$). This garnet type exhibits weak diffusion and irregular zoning with grossular-almandine-rich domains. The spessartine content is minor; pyrope is negligible (total <4 mol%); and uvarovite is almost nil in all the garnet crystals (Table 1; Fig. 3).

Andradite is the most abundant end-member in the garnets analyzed. Based on EPMA results, andradite content decreases towards the rim in isotropic garnets and grossular and almandine compositions vary antithetically with andradite (Fig. 4). Similarly, the Fe^{2+} (almandine content) increases and Fe^{3+} (andradite content) decreases from the cores to the rims (Fig. 5). The variation in the sum of the andradite, grossular and almandine components in the isotropic garnets is smooth from the cores to the rims. As shown in Fig. 4, Garnet III exhibits considerable variation in its composition. There is a distinct decrease in the andradite component and increase in the grossular-almandine components, which correspond to a discrete gray colored domain in the garnet and shows an optically anisotropic feature.

Only garnet III demonstrates noticeable variation from the core to the rim. The other garnets do not vary noticeably and remain relatively constant in composition. However, Si, Fe^{2+}, Mn, Mg, Cu and Ti content increases and Al, Fe^{3+}, Ca and Ni decreases from core to rim. Fig. 6 shows similarities and differences of the garnet crystals between the Astamal skarn and the Cananea, Mission, Yerington, Bingham and Twin Butte skarn deposits (Einaudi, 1982).

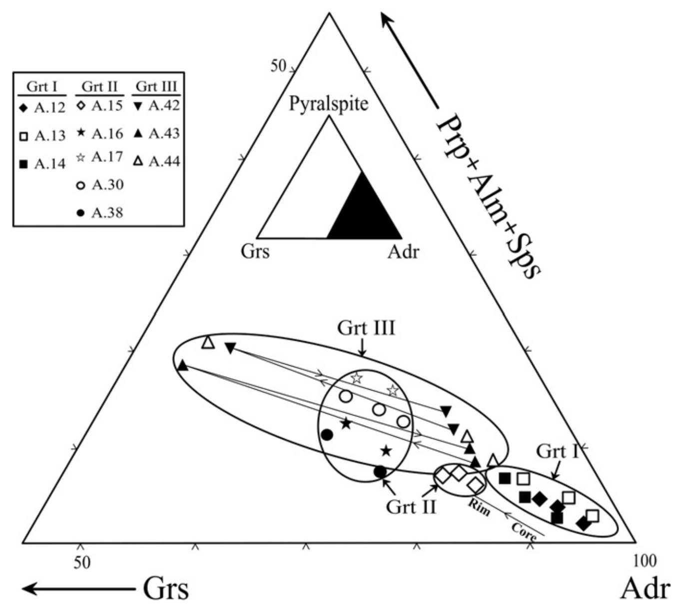

Fig 3. Composition of the Astamal skarn garnets in the Andradite-Grossular-Pyralspite ternary diagram. Pyralspite includes pyrope, almandine and spessartine and arrows indicate the growth trends in the garnets from core to rim (the trend of A44 is the same as samples A43 and A42). EPMA data are given in Table 1. Abbreviations: Adr = andradite, Alm = almandine, Grs = grossular, Grt = garnet, Prp = pyrope, and Sps = spessartine.

5.1. Trace elements

Garnets have the general chemical formula $X_3Y_2Z_3O_{12}$ (eight formula units per basic cell). Site X corresponds to eight-fold (dodecahedral) coordination of metal in the 24c position ($X = Ca^{2+}$, Fe^{2+}, Mg^{2+} or Mn^{2+}); Y corresponds to six-fold (octahedral) coordination in the 16a position ($Y = Al^{3+}$, Cr^{3+} or Fe^{3+}); and Z to four-fold (tetrahedral) coordination (largely Si) in the 24d position (Barcova et al., 2002).

Garnet II has distinct Cu and Ni compositions. Their values are given in Table 2 for comparison with Cu and Ni content of garnet from the Sungun, Mazraeh and Tikmeh-Dash skarn deposits (Karimzadeh Somarin, 2004). Copper content shows an increase towards the rims of the garnets; conversely, Ni values show a minor decrease towards the rims (Fig. 7a and e, respectively). Furthermore, Cu content is elevated with increasing proportion of the almandine end-member (Fig. 7b) and depleted with increasing proportion of the andradite end-member and total Fe (Fig. 7c and d, respectively). These changes are accompanied by lower Ni content with increasing almandine content (Fig. 7f) and elevated Ni with increasing andradite content and total Fe (Fig. 7g and h, respectively).

6. Discussion and interpretation

Garnet growth reflects the interplay of temperature changes and fluid infiltration of the host rocks (e.g., Jamtveit, 1997; Meinert et al., 2005). Coarse-grained garnets in skarn deposits are usually formed in the periphery of the associated intrusive bodies. However, Einaudi et al. (1981) suggested that the dimensions of garnet grains are more closely associated with the rate of fluid flow and equilibrium conditions between the hydrothermal fluids and wall rock. Relatively high rates of

Fig 2. Photomicrographs of the Astamal skarn samples: (a) replacement of euhedral coarse-grained isotropic garnet (garnet I) by calcite and quartz both in the rim and the core exhibits intensive alteration. (b) Magnetite replacing garnet I rims within the un-mineralized zone (plane-polarized light). (c and d) Anhedral to subhedral isotropic garnets (garnet II) in a calcite matrix (c under cross-polarized transmitted light; d under non-polarized transmitted light). (e and f) Coarse-grained garnet (garnet III) showing an irregular zoning with grossular-almandine-rich discrete and recognizable domains (grayish color domains within the garnet; e under cross-polarized transmitted light; f under non-polarized transmitted light). Abbreviations: Aln = Allanite, Cal = Calcite, Chl = Chlorite, Ep = Epidote, Grt = Garnet, Opq = Opaque minerals, Pc = Pistacite Qz = Quartz. Abbreviations from Whitney and Evans (2010).

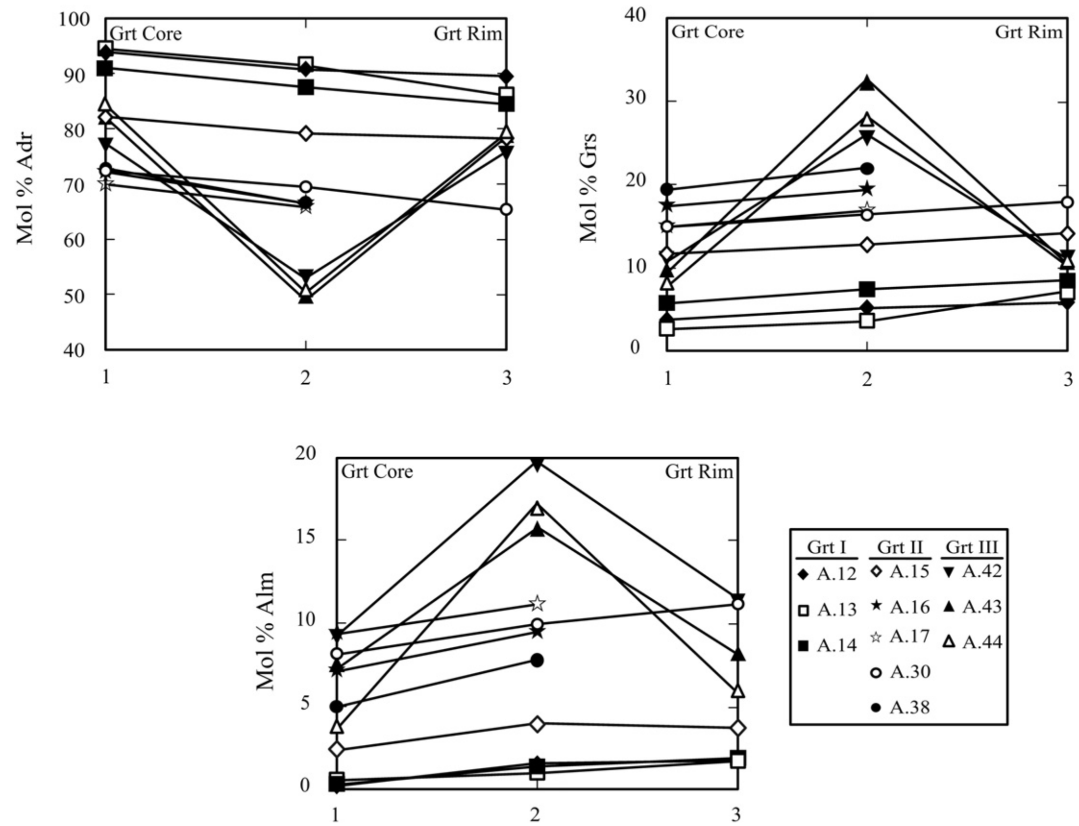

Fig 4. Chemical zonation pattern of the Astamal garnets end-member displaying considerable variation in garnet III and slight variation for garnets I and II in the terms of Adr-Grs-Alm end-members from the core (1 in X axis) to the rim (3 in X axis).

fluid flow result in supersaturation of elements such as Fe, Mg, Al and Ca. In magmatic hydrothermal environments situated distal to the intrusive bodies (such as the Astamal skarn), fluid movement is relatively limited and consequently the degree of supersaturation is limited. In these conditions, crystals grow slowly and form coarser grains.

The garnets of the Astamal skarn are predominantly in an andradite-grossular solid solution. The growth is characterized by a continuous outward decrease of X_{Adr} and X_{Fe} [$=Fe/(Fe + Mg)$] and an increase of X_{Grs} and X_{Alm} (i.e., there is a positive correlation between the almandine and the grossular components). Einaudi and Burt (1982) suggested that almandine content increases with increasing substitution of Al for Fe^{3+} (increasing Grs/Adr). The observed increase in almandine content towards the edge of the crystals could also be due to an increase in the Fe^{2+} activity and a decrease in fO_2 during garnet growth.

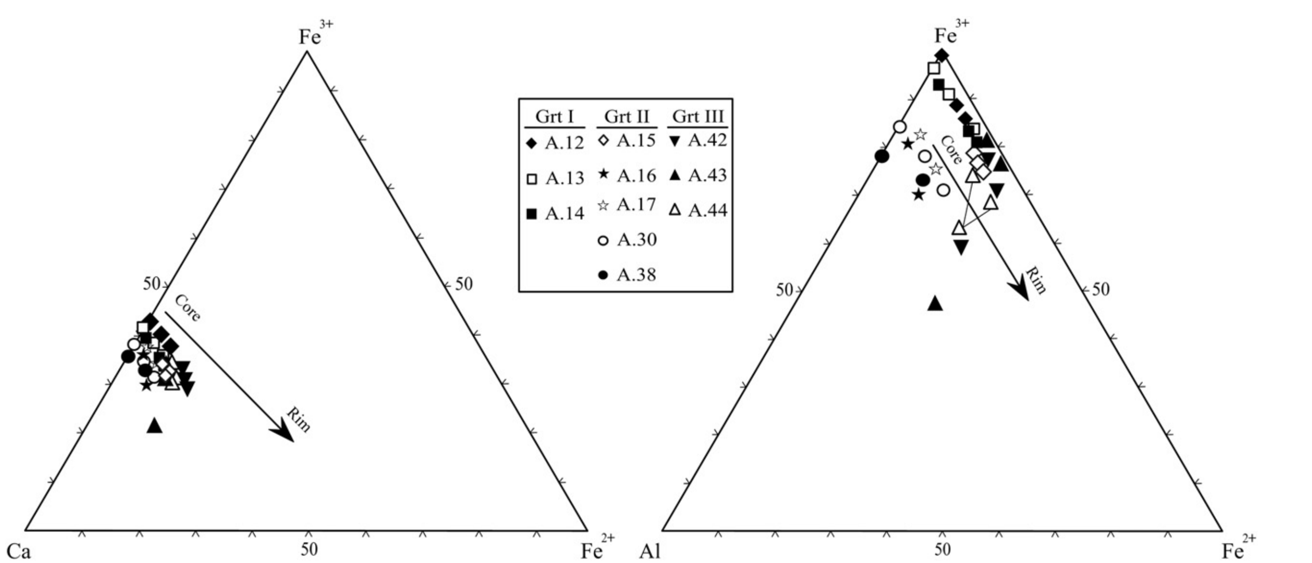

Fig 5. Ternary diagrams showing Fe^{2+} and Fe^{3+} variation of garnets from the Astamal skarn in terms of Fe^{3+}-Fe^{2+}-Ca and Fe^{3+}-Fe^{2+}-Al (atomic). Arrows indicate the direction of zoning from the core to the rim (the trends of A42 and A43 are the same as that in sample A44).

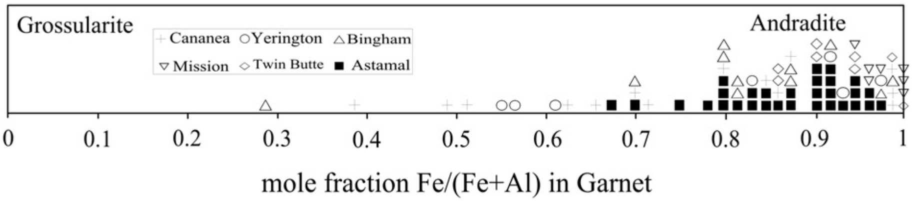

Fig 6. Comparison of garnet composition from the Astamal skarn with some other skarn deposits in terms of Fe/(Fe + Al) mole fraction (Einaudi, 1982).

The Cu^{2+} content is elevated with an increase of the almandine component and decreases with an increase of the andradite component. According to the principles of elemental substitution (Goldschmit, 1954), divalent cations such as Cu^{2+} can be substituted easily for Fe^{2+} during the alteration processes. Hence, it is concluded that the almandine structure (with more Fe^{2+}) is more suitable than andradite and grossular to host divalent cations such as Cu^{2+}. Conversely, Ni content shows a positive correlation with increasing andradite abundance and total Fe because Ni^{2+} substitutes for Fe^{3+} in the Y position (octahedron). These compositional features of the garnets and the presence of chalcopyrite and dense magnetite in the study area (Baghban, 2013), suggest that Cu and Ni were present in both the prograde and retrograde mineral-forming hydrothermal fluids. Generally, the partitioning of trace elements between the metasomatic fluid and the garnet is complex and strongly constrained by crystal chemistry, crystal-liquid equilibrium (e.g., P, T, and fluid composition), and kinetic effects such as growth rate and surface adsorption (Chernoff and Carlson, 1999; Smith et al., 2004).

In the Astamal skarn, garnets I and II are generally isotropic and there is no specific zoning along the growth lines, whereas garnet III exhibits weak diffusion and irregular zoning. The formation of a hornfelsic cap (Baghban et al., 2015) likely prevented the penetration of cold meteoric fluids into the system, which may have resulted in the formation of homogenous garnets. This is because the hornfelsic cap may have acted as an insulator that prevented the loss of heat from the system. Garnets with zoning patterns indicate an episode of rapid cooling from the metamorphic/metasomatic peak during crystallization. This rapid cooling rate may be due to a rapid uplift and unroofing of the hydrothermal system. Spear (2004) suggested that the most important model parameters for determining the cooling rate are thrust velocity and ramp angle; steeper ramps and faster thrusting rate result in faster cooling. A thrusting rate of several cm/year or faster along a thrust fault with a ramp of 10° or more will produce a garnet cooling rate >100 °C/Ma. On the contrary, Fernando et al. (2003) estimated a slow cooling rate of 1–5 °C/Ma for garnets with retrograde diffusion zoning. Therefore, with the assumption that garnet formation is contemporaneous with or shortly after emplacement of the Qara-Dagh batholith (of Oligocene age) and that there was also minimal penetration of cold meteoric fluids into the system, a moderate cooling rate of 10–20 °C/Ma for 20–30 Ma is approximated for the Astamal garnets.

The lack of significant zoning in garnets I and II can be explained by increased diffusion rates within the mineral at high temperatures (Dietvorst, 1982). Chakraborty and Ganguly (1990) showed at under these conditions, diffusion tends to reduce existing chemical profiles and thereby homogenize the garnets. These authors also concluded that Ca is the slowest divalent cation to diffuse in garnets (i.e., the intrinsic diffusion coefficient of Ca is smaller than those of Fe and Mg). One possible explanation for the slower diffusion of Ca may be the larger size of the Ca cation compared to Mg and Fe. As presented in Table 1, FeO values show a large decrease in samples A42, A43 and A44 (~2 wt%), compared to the CaO values (~5 wt%) in the same samples. Hence, the discrete domains of higher grossular-almandine content in garnet III can be explained by the low diffusivity of Ca compared to Fe and substitution of Al^{3+} for Fe^{3+} at high temperatures. The presence of high temperature minerals such as wollastonite and cordierite in the study area (Baghban et al., 2015) confirm that these garnets formed at temperatures >550 °C. Fig. 8 shows the stability field of the andradite-grossular solid solution at $XCO_2 = 0$ to 1. In most skarns, XCO_2 varies from initial values of 0.2 to 0.5 (Einaudi et al., 1981). However, these values can increase slightly when wollastonite is present. Andradite is stable in relatively low XCO_2 conditions, but its decomposition to hedenbergite, calcite and magnetite, and the subsequent decomposition of hedenbergite to actinolite, calcite and quartz is concomitant with increasing of XCO_2 (Uchida, 1983). Therefore, XCO_2 values are believed to be relatively high in both the prograde and retrograde alteration stages. Based on the EPMA results, the compositional variation of the Astamal garnets are $Adr_{94.3–48.8}$ $Grs_{32.4–2.7}$ $Alm_{19.9–0.2}$. Hence, based on T-XCO_2 diagrams (Fig. 8), the garnets likely formed at temperatures between 500–560 °C. Therefore, it can be concluded that the garnets of the Astamal skarn formed at high temperatures with low/moderate cooling rate.

7. Conclusion remarks

(1) Garnet is the dominant mineral in the Astamal skarn and is present in three forms: strongly altered euhedral coarse-grained isotropic garnets (garnet I); slightly altered anhedral to subhedral brecciated isotropic garnets (garnet II) and mildly altered subhedral coarser-grained garnets with weak diffusion and irregular zoning (garnet III). All three garnet types altered to a fine-grained, dark-gray disseminated allanite which is rarely well documented in other skarn deposits.
(2) The garnets likely formed at high temperatures (500–560 °C) with a low/moderate cooling rate (10–20 °C/Ma).
(3) EPMA shows that:

(a) The garnets are of andradite-grossular solid solution composition, have high Fe/(Fe + Al) ratios and display a monotonic decrease in the andradite content and increase in the grossular and almandine contents towards the rim.
(b) Garnet II has discernible Cu and Ni contents. Copper (II) content shows a positive correlation with almandine abundance and a negative correlation with andradite abundance and total Fe because of the higher concentration of Fe^{2+} in almandine and the substitution of Fe^{2+} by Cu^{2+}. Nickel (II) content shows a positive correlation with andradite abundance and total Fe and

Table 2
Comparison of garnet Cu and Ni concentrations of some skarn deposits in NW Iran (Sungun, Mazraeh and Tikmeh Dash data compiled from Karimzadeh Somarin, 2004).

Area	Cu	Ni
Astamal Fe-LREE skarn	0–1997	0–1283
Sungun Cu porphyry-skarn	60–670	8–19
Mazraeh Cu-Fe skarn	280–680	7–12
Tikmeh Dash Fe-Cu skarn	16–25	5–8

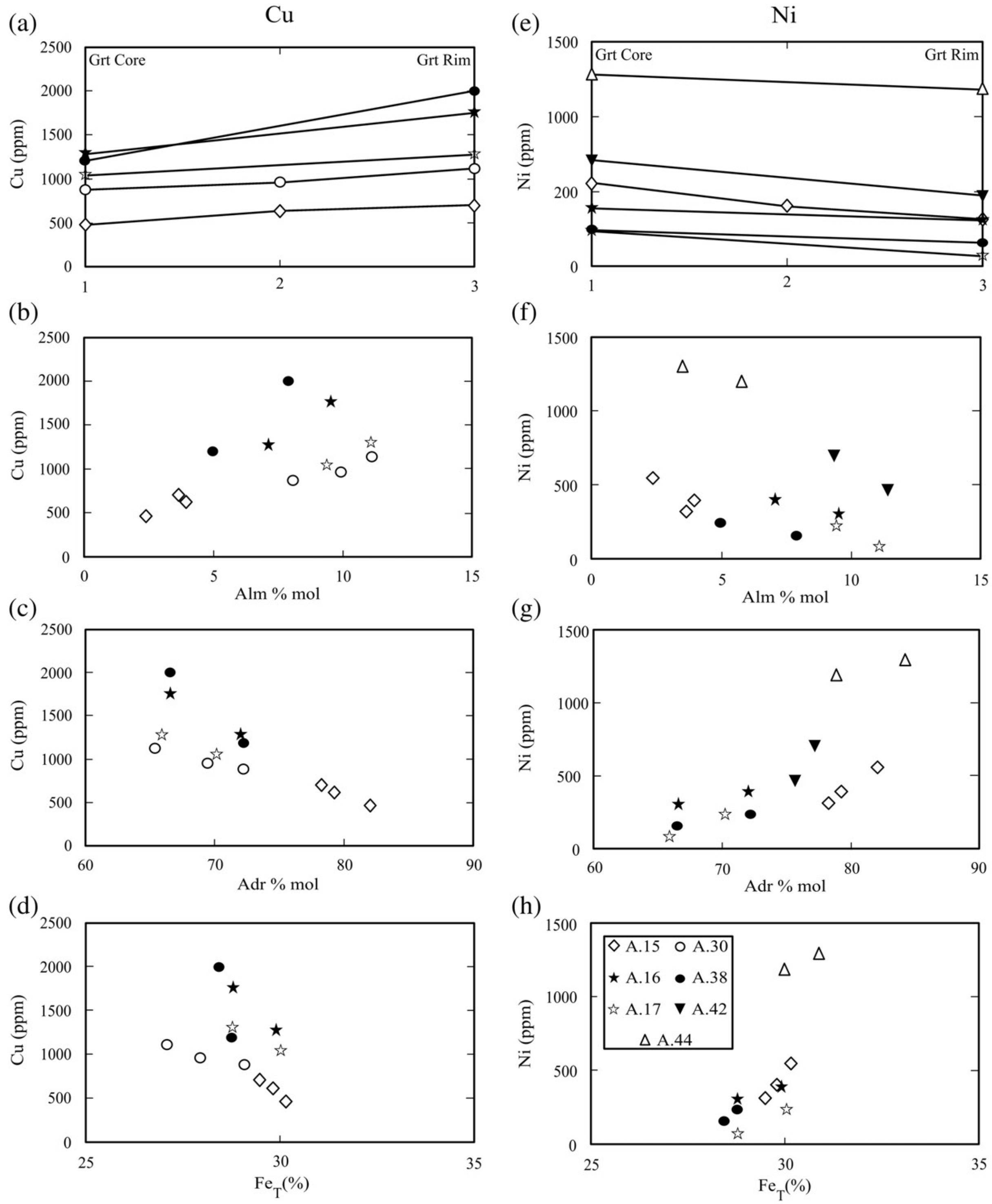

Fig 7. Bivariate diagrams for Cu and Ni contents of the Astamal garnets showing (a) Cu variation from core to rim; (b) positive correlation of Cu with almandine values; (c) negative correlation of Cu with andradite values; (d) negative correlation of Cu with total Fe; (e) Ni variation from core to the rim; (f) negative correlation of Ni with almandine values; (g) positive correlation of Ni with andradite values; and (h) positive correlation of Ni with total Fe.

a negative correlation with almandine abundance. This can be explained by the replacement of Fe^{3+} by Ni^{2+} in the Y position (octahedron).

(c) Discrete grossular-almandine rich domains in garnet III show a steep gradient, changing by as much as 23 mol% grossular to 13 mol% almandine over a distance of a millimeter because of the substitution of Fe (III) by Al (III) and low diffusivity of Ca compared to Fe at high temperatures.

Acknowledgments

Sincere gratitude goes to Masoud Baghban for his assistance and insightful discussions throughout the course of this study. We thank Dr. Selina Wu for helping edit the English in the manuscript. The manuscript also benefitted from extensive reviews by Dr. Xue-Ming Yang and one anonymous journal reviewer. Associate Editor Dr. Leon Bagas contributed significantly to improve the manuscript.

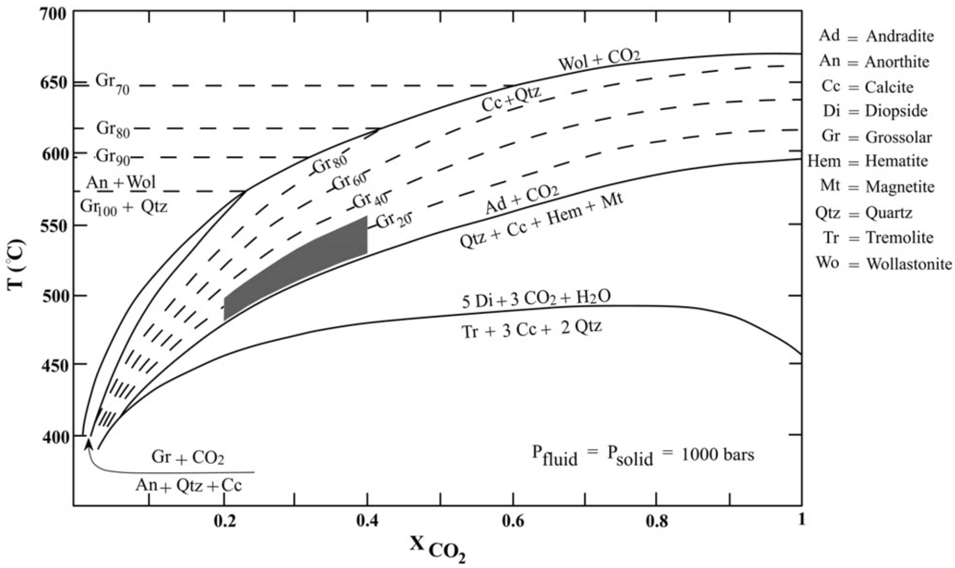

Fig 8. T-XCO_2 diagram at $P_{fluid} = 1000$ bars (adapted from Sweeney, 1980). Gr_{100} is pure Ca-Al garnet (grossular); Ad is pure Ca-Fe garnet (andradite); and Gr_{20}-Gr_{80} represents andradite-grossular solid solution. The gray reticular-hatched area in the diagram is the stability field of the garnets from the Astamal skarn.

References

Baghban, S., 2013. Genesis, mineralogy, and geochemistry of the Astamal Iron skarn, NE of Kharvana, Eastern Azarbaijan province, Iran. Unpublished M.Sc. thesis, Tabriz University, 185 pp. (in Persian with English abstract).

Baghban, S., Hosseinzadeh, M.R., Moayyed, M., Mokhtari, M.A.A., Gregory, D.D., 2015. Geology, mineral chemistry and formation conditions of calc-silicate minerals of Astamal Fe-LREE distal skarn deposit, Eastern Azarbaijan Province, NW Iran. Ore Geol. Rev. 68, 79–96.

Barcova, K., Mashlan, M., Martinec, P., 2002. Mössbauer study of the thermal behavior of garnets used in high-energy water jet technologies. Hyperfine Interact. 139-140, 463–569.

Chakraborty, S., Ganguly, J., 1990. Compositional zoning and cation diffusion in garnets. In: Ganguly, J. (Ed.), Diffusion, Atomic Ordering and Mass Transport: Selected Problems in Geochemistry. Advanced in Physical Geochemistry Vol. 8, pp. 120–175.

Chernoff, C.B., Carlson, W.D., 1999. Trace element zoning as record of chemical disequilibrium during garnet growth. Geology 27, 555–558.

Deer, W.A., Howie, R.A., Zussman, J., 1992. An Introduction to the Rock-forming Minerals. second ed. Longman Scientific and Technical, Essex.

Dietvorst, E.J.L., 1982. Retrograde garnet zoning at low pressure in metapeletic rocks from kemio, SW Finland. Contrib. Mineral. Petrol. 79, 37–45.

Einaudi, M.T., 1982. General features and origin of skarns associated with porphyry copper plutons. Advances in Geology of Porphyry Copper Deposits, Southwestern North America, Tucson. University of Arizona Press, pp. 185–209.

Einaudi, M.T., Burt, D.M., 1982. Introduction terminology, classification and composition of skarn deposits. Econ. Geol. 77, 745–754.

Einaudi, M.T., Meinert, L.D., Newberry, R.J., 1981. Skarn Deposits (Economic Geology 75th Anniversary) pp. 317–391.

Fernando, G.W.A.R., Hauzenberger, C.A., Baumgartner, L.P., Hofmeister, W., 2003. Modeling of retrograde diffusion zoning in garnet: evidence for slow cooling of granulites from the Highland Complex of Sir Lanka. Mineral. Petrol. 78, 53–71.

Gaspar, M., Knaach, C., Meinert, L., Moretti, R., 2008. REE in skarn systems: A LA-ICP-MS study of garnets from the Crown Jewel gold deposit. Geochim. Cosmochim. Acta 72, 185–205.

Goldschmit, V.M., 1954. Geochemistry. Clarendon Press, Oxford.

Ismail, R., Ciobanu, C.L., Cook, N.J., Teale, G.S., Giles, D., Mumm, A.S., Wade, B., 2014. Rare earths and other trace elements in minerals from skarn assemblages, Hillside iron oxide–copper–gold deposit, Yorke Peninsula, South Australia. Lithos 184, 456–477.

Jamtveit, B., 1997. Crystal growth and intercrystalline zonation patterns in hydrothermal system. In: Jamtveit, B., Meakin, P. (Eds.), Growth and Dissolution and Pattern Formation in GeosystemsAmerican Mineralogist Vol. 76. Netherland Kluwer Academic, pp. 65–82.

Jamtveit, B., Hervig, R.L., 1994. Constraints on transport and kinetics in hydrothermal systems from zoned garnet crystals. Science 263, 505–508.

Jansson, N.F., Allen, R.L., 2013. Timing and setting of skarn and iron oxide formation at the Smältarmossen calcic iron skarn deposit, Bergslagen, Sweden. Mineral. Deposita 48, 313–339.

Karimzadeh Somarin, A., 2004. Garnet composition as an indicator of Cu mineralization: evidence from skarn deposits of NW Iran. J. Geochem. Explor. 81, 47–57.

Karimzadeh Somarin, A., 2010. Garnetization as a ground preparation process for copper mineralization: evidence from the Mazraeh skarn deposit, Iran. Int. J. Earth Sci. 99, 343–356.

Meinert, L.D., Dipple, G.M., Nicolescu, S., 2005. World Skarn Deposits (Economic Geology 100th Anniversary) pp. 299–336.

Mokhtari, M.A.A., Hosseinzadeh, R., 2013. General Exploration of Astamal Iron Mineralization, NE of Kharvana. Geological Survey of Iran (86 pp. (in Persian with English abstract)).

Nicolescu, S., Cornell, D.H., Sodervall, U., Odelius, H., 1998. Secondary ion mass spectrometry analysis of rare earth elements in grandite garnet and other skarn related silicates. Eur. J. Mineral. 10, 251–259.

Peng, H.J., Zhang, Ch.Q., Mao, J.W., Santosh, M., Zhou, Y.M., Hou, L., 2015. Garnets in porphyry–skarn systems: a LA–ICP–MS, fluid inclusion, and stable isotope study of garnets from the Hongniu–Hongshan copper deposit, Zhongdian area, NW Yunnan Province, China. J. Asian Earth Sci. 103, 229–251.

Smith, M.P., Hendersen, P., Jeffries, T.E.R., Long, G., Williams, C.T., 2004. The rare earth elements and uranium in garnets from the Benin and Dubhaich aureole, Sky, Scotland, UK, Constrain on processes in a dynamic hydrothermal system. J. Petrol. 45, 457–484.

Spear, F.S., 2004. Fast cooling and exhumation of the Valhalla metamorphic core complex, Southeastern British Columbia. Int. Geol. Rev. 46, 1–17.

Sweeney, M.J., 1980. Geochemistry of garnets from the North Ore shoot, Bingham district, Utah. Unpublished M.Sc. thesis, University of Utah, 154 pp.

Uchida, E., 1983. Grunerite from the Shinyama ore deposit, Kamaishi mine, Japan. Can. Mineral. 21, 517–528.

Whitney, D.L., Evans, B.W., 2010. Abbreviations for names of rock-forming minerals. Am. Mineral. 95, 185–187.

Whitney, P.R., Olmsted, J.F., 1998. Rare earth element metasomatism in hydrothermal systems: the Willsboro-Lewis wollastonite ores, New York, USA. Geochim. Cosmochim. Acta 62, 2965–2977.